Spherical aberration correction in nonlinear microscopy and optical ablation using a transparent deformable membrane

P. S. Tsai, B. Migliori, K. Campbell, and T. N. Kim
Department of Physics, University of California at San Diego, La Jolla, California 92093, USA

Z. Kam
Molecular Biology of the Cell, Weizmann Institute of Science, Rehovot, 761002, Israel

A. Groisman[a),b)]
Department of Physics, University of California at San Diego, La Jolla, California 92093, USA

D. Kleinfeld[a),c)]
Department of Physics, University of California at San Diego, La Jolla, California 92093, USA and
Graduate Program in Neurosciences, University of California at San Diego, La Jolla, California 92093, USA

(Received 7 August 2007; accepted 10 October 2007; published online 5 November 2007)

We describe the design and utilization of a deformable membrane to minimize the negative spherical aberration that occurs when a standard water-dipping objective is used to focus within a higher-index sample. In connection with two-photon laser scanning microscopy, we demonstrate twofold improved axial resolution of structures as deep as 1 mm in gels and brain tissue. In conjunction with plasma-mediated ablation, we demonstrate enhanced production of optical damage deep within a glass substrate. The present method provides a simple and inexpensive correction for a limited yet important class of optical aberrations. © *2007 American Institute of Physics*. [DOI: 10.1063/1.2804014]

An essential requirement of nonlinear optical techniques is the ability to achieve axial confinement of the focus. Within biology, two photon laser scanning microscopy[1] (TPLSM) is used to image fluorescent structures deep within tissue.[2,3] It is invariably performed through water-dipping objectives that have a high numerical aperture (NA) and long working distance. These lenses are designed to image at the surface of the tissue. Thus, their resolution deteriorates with increasing depth in the tissue as a result of expansion of the focal region by spherical aberration. Within engineering, plasma-mediated ablation with femtosecond laser pulses[4] is used to modify material for three-dimensional data storage,[5] waveguide writing,[6,7] and microchannel fabrication.[8] Oil-immersion objectives can be used to avoid spherical aberration in glass and plastic substrates. Yet, with one exception,[9] these objectives do not have working distances greater than 200 μm. Ablation at larger depths in glass and plastic, as well as manipulation of biological tissue with plasma mediated ablation,[10–13] requires the use of water-dipping objectives.

When a water-dipping objective is used to image within a higher-index material, i.e., for $n>1.33$, refraction occurs at the water-to-sample interface and induces negative spherical aberration of the beam.[14] Thus, marginal rays focus deeper than paraxial rays and the focus is increasingly degraded with increasing depth into the sample. To counteract this effect, the radial phase profile of the beam can be modified to compensate for the differences between the marginal and paraxial paths. Toward this end, we demonstrate a solution that makes use of a transparent deformable membrane.

The membrane is 1.5 mm thick and is fabricated from polydimethyl siloxane (PDMS) (RTV615, General Electric). Prior to curing, the PDMS prepolymer is leveled with the guidance of an interferometer to ensure an optical flatness of $<0.003\%$ (rise/run), i.e., less than one wavelength over a 12 mm aperture. The membrane is affixed to one face of an acrylic mount and a glass window is affixed to the other face of the mount (Supplemental Information) [Fig. 1(a)]. The mount is held in a linear translation stage [Fig. 1(b)]. Application of vacuum to the interior of the mount pulls the membrane inward, so that it acquires the shape of a meniscus lens [Fig. 1(c)]. Vacuum with gauge pressures that range from

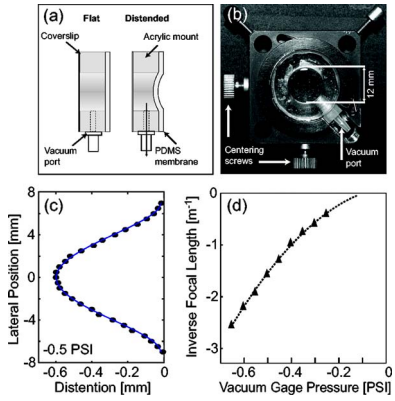

FIG. 1. (Color online) Membrane and mount for aberration correction. (a) Cutaway illustration of the mounted flat and distended membrane. (b) Photograph of the completed assembly. (c) The measured distention of the membrane, z, as a function of radial position r at a gauge pressure of −0.5 psi. Here and in all other displayed graphs, each datum represents an average of three measurements. The data were fitted with the function $z=\eta[1-(r/r_o)^2]^2$, where $\eta=0.60$ mm and $r_o=7.04$ mm. (d) Plot of the effective focal length of the distended membrane vs vacuum pressure. The focal length was determined by imaging a filament with the membrane in tandem with an $f=+200$ mm fixed lens. The curve is parabolic fit to the data.

[a)]Author to whom correspondence should be addressed.
[b)]TEL: 858-822-1838. Electronic mail: agroisman@ucsd.edu
[c)]TEL: 858-822-0342. Electronic mail: dk@physics.ucsd.edu

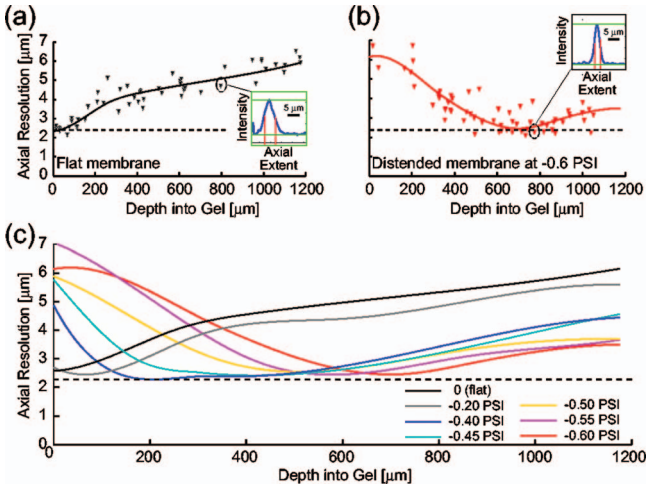

FIG. 2. (Color) On-axis axial resolution from TPLSM imaging with a 40 ×, 0.8 NA, water-dipping objective. Resolution with the (a) membrane flat and (b) distended. The FWHM was measured from images of beads that were embedded in an $n=1.42$ test gel (see insets). The curves represent cubic spline fits to data. (c) Curves that represent data from various dilations of the membrane. The insets are plots of axial cross sections of the beads, used to define resolution.

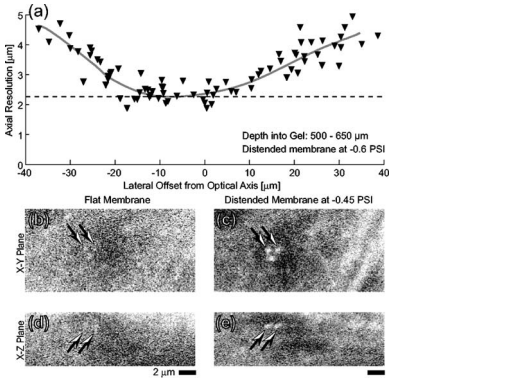

FIG. 3. Off-axis axial resolution from TPLSM imaging with a 40×, 0.8 NA, water-dipping objective. (a) Resolution vs lateral position relative to the optical axis. [(b)–(e)] Endogenously labeled mitochondria in a sucrose-cleared section of mouse brain that was imaged with TPLSM at a depth of 700 μm. The *X-Z* planes are derived from *X-Y* image stacks. Mitochondria (yellow arrows) that are barely discernble with the membrane flat [panels (b) and (d)] are clearly visible with the membrane distended at −0.5 psi gauge pressure [panels (c) and (e)].

−0.3 to −0.7 psi results in effective focal lengths between $f=-2000$ and −400 mm, respectively, near the optical axis of the dilated membrane [Fig. 1(d)].

Two photon laser scanning microscopy and plasma-mediated ablation were performed with a previously described two photon microscope,[15,16] modified for concurrent ablation,[17] at a center wavelength of 800 nm. All data were obtained with a 0.8 NA, 40 times magnification water-dipping objective (440095, Zeiss) with a 3.6 mm working distance, and a back aperture of 6.6 mm in diameter that is located 34.9 mm from the back shoulder of the objective. The membrane was located approximately 5 mm behind the shoulder. Test samples for TPLSM consisted of 0.2 μm diameter fluorescent beads (17151-10, Polysciences) suspended in a gel of 60% (w/v) sucrose and 1% (w/v) agarose (A4018, Sigma) and topped with a No. 0 coverslip; this mimics the imaging conditions in cleared fixed tissue in which 60% (w/v) sucrose solution $(n=1.42)$ is used as an index-matching agent.[18,19] Axial resolution was determined algorithmically using routines written in MATLAB (Supplemental Information) and is reported as the full width at half maximum (FWHM) intensity. Brain tissue was prepared as 1 mm thick sections of paraformaldehyde-fixed cortex that was permeabilized with 1% (v/v) Triton X-100, cleared by equilibration with 60% (w/v) sucrose, and mounted under a No. 0 coverslip.

The on-axis axial resolution with the membrane flat was 2.2 μm at the surface, equal to the diffraction-limited value, and degraded to greater than twice that value at depths of 700 μm and beyond [Fig. 2(a)]. Dilation of the membrane at gauge pressure of −0.6 psi restored the axial resolution to the original value of 2.2 μm [Fig. 2(b)]. Variable dilation of the membrane provides aberration compensation continuously across depths of 0–1 mm [Fig. 2(c)]. Further, use of the membranes provided an axial resolution of 2.5 μm over a field with a lateral extent of 35 μm for depths up to 650 μm [Fig. 3(a)].

As an application of the improved resolution achieved with the deformable membrane, we imaged the fluorescence from cyan fluorescent protein that is expressed exclusively in neuronal mitochondria of a strain of transgenic mice.[20] Mitochondria are less than 1 μm in diameter. At a depth of 700 μm through brain tissue, the individual mitochondria are difficult to discern in both lateral [Fig. 3(b)] and transverse [Fig. 3(d)] planes of TPLSM images. Compensation with the membrane provides greatly enhanced image contrast and individual mitochondria are clearly resolved in both projections [Figs. 3(c) and 3(e)].

As a second application of the membrane, we attempted to ameliorate the axial elongation of the damage zone in plasma-mediated ablation. Glass samples were prepared from two slides, each 1 mm in thickness, that were pressed side to side to form a continuous sheet with a split [Fig. 4(a)]. Damage was produced at different locations, defined by their depth and the energy per pulse, along a line that paralleled the split with a separation distance of about 70 μm. The depths varies from 0 to 800 μm below the top face and we used a range of average pulse energies that extended both above and below the threshold energy for damage. Approximately 2000 pulses were delivered for each location. Damage was visualized through the side face [Fig. 4(b)] (Supplemental Information). At a depth of 500 μm, damage was just barely discernible using a flat membrane and pulse energies of 0.4 μJ. In contrast, aberration correction with the distended membrane led to damage that is readily discerned [Fig. 4(c)]. At pulse energies of 0.3 μJ, the uncompensated condition yielded no discernible damage, while the compensated condition continued to produce clearly visible damage [Fig. 4(d)].

Plasma-mediated ablation with the membrane in the flat state and a pulse energy of 7 μJ yielded damage with an increasing axial extent as a function of depth into the glass [Fig. 4(e)]. Compensation by dilation of the membrane reduced the axial extent of the damage region upward of 50% for the same pulse energy. For example, the axial extent of damage at a depth of 800 μm was reduced from 38 to 20 μm with the membrane distended at a gauge pressure of −0.6 psi [Fig. 4(f)]. Continuous variation of the pressure allows for optimal compensation at intermediate depths (data not shown).

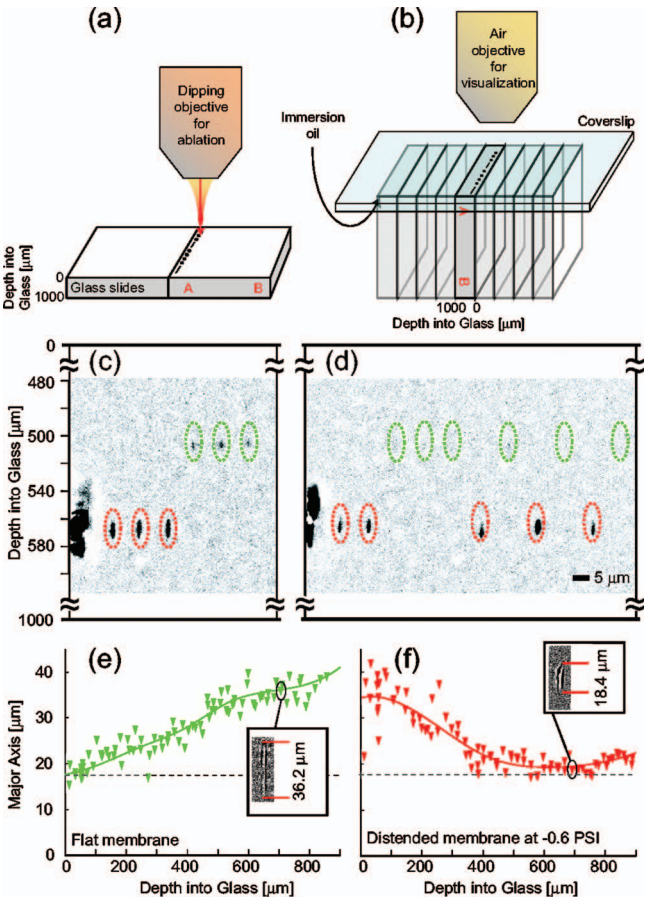

FIG. 4. (Color) Aberration correction for plasma-mediated ablation in glass. (a) Schematic of the configuration for ablation. (b) Schematic of the configuration for damage visualization. Immersion oil between a no. 0 coverslip and the unpolished side face provided optical uniformity. Multipulse damage from (c) 0.4 μJ and (d) 0.3 μJ pulses focused approximately 500 μm into glass; green ellipses indicate foci with the membrane flat while red ellipses indicate foci with the membrane distended at −0.5 psi gauge pressure. Axial damage with the membrane (e) flat and (f) distended at −0.6 psi gauge pressure. Images were obtained under bright-field illumination with a 20×, 0.75 NA air objective.

Geometric ray tracing through the distended membrane, which was modeled as a thin circular plate with a clamped edge[21] [Fig. 1(c)], confirmed that its central area acts as a diverging lens. Further, the membrane exhibits negative spherical aberration, i.e., the paraxial rays have a shorter focus than the marginal rays. The dipping objective was modeled as a planoconvex aspheric lens formulated to generate a perfect on-axis focus in water for a collimated input. We found that both changes to the input beam by the distended membrane, i.e., the divergence of the beam and the negative spherical aberration, compensate for the negative spherical aberration induced by imaging deep into the high index sample with the dipping objective (Supplemental Material).

To summarize, we designed and fabricated a deformable membrane (Fig. 1) that yielded a twofold enhancement of axial resolution for TPLSM at depths of nearly 1 mm in test samples (Fig. 2). For Nyquist-limited sampling with a 0.8 NA objective, we obtained 2.5 μm axial resolution over a 200×200 pixel (35×35 μm^2) field at an image depth of 650 μm (Fig. 3). For plasma-mediated ablation, we achieved a twofold improvement in axial confinement (Fig. 4). Further, aberration compensation can extend the depth at which ablation can be achieved when laser power is limited.

The present device is both simpler and less costly to fabricate than fully programmable adaptive optics, such as deformable mirrors[22–24] and liquid-crystal phase shifters.[25] While the latter devices offer angular as well as radial correction, and thus can compensate for phase differences induced by variations within the sample, only radial corrections are needed to compensate for spherical aberration. Lastly, the realization of deformable membranes that are optimized for different objectives merits investigation.

We thank Thomas Misgeld for the gift of transgenic mice, Olympus America Inc. for the loan of an objective, and Carl Zeiss Inc. for details on the dipping lens. This work was funded by grants from the DARPA Center for Optofluidic Integration, the NIH (RR021907 and EB003832), and the NSF (DBI 0455027).

[1]W. Denk, J. H. Strickler, and W. W. Webb, Science **248**, 73 (1990).
[2]F. Helmchen and W. Denk, Nat. Methods **2**, 932 (2005).
[3]W. Denk and K. Svoboda, Neuron **18**, 351 (1997).
[4]M. Lenzner, J. Kruger, S. Sartania, Z. Cheng, C. Spielmann, G. Mourou, and F. Kautek, Phys. Rev. Lett. **80**, 4076 (1998).
[5]M. H. Hong, B. Luk'yanchuk, S. M. Huang, T. S. Ong, L. H. Van, and T. C. Chong, Appl. Phys. A: Mater. Sci. Process. **79**, 791 (2004).
[6]C. B. Schaffer and E. Mazur, *Optics and Photonics News* (Optical Society of America, Washington, D. C., 2001), Vol. 12, pp. 20–23.
[7]R. Osellame, N. Chiodo, G. Della Valle, S. Taccheo, R. Ramponi, G. Cerullo, A. Killi, U. Morgner, M. Lederer, and D. Kopf, Opt. Lett. **29**, 1900 (2004).
[8]T. N. Kim, K. Campbell, A. Groisman, D. Kleinfeld, and C. B. Schaffer, Appl. Phys. Lett. **86**, 201106 (2005).
[9]A. M. Kowalevicz, V. Sharma, E. P. Ippen, J. G. Fujimoto, and K. Minoshima, Opt. Lett. **30**, 1060 (2005).
[10]N. Nishimura, C. B. Schaffer, B. Friedman, P. S. Tsai, P. D. Lyden, and D. Kleinfeld, Nat. Methods **3**, 99 (2006).
[11]M. F. Yanik, H. Cinar, H. N. Cinar, A. D. Chisholm, Y. Jin, and A. Ben-Yakar, Nature (London) **432**, 822 (2004).
[12]T. Juhasz, H. L. Loesel, R. M. Kurtz, C. Horvath, J. F. Bille, and G. Mourou, IEEE J. Sel. Top. Quantum Electron. **5**, 902 (1999).
[13]H. Lubatschowski, G. Maatz, A. Heisterkamp, U. Hetzel, W. Drommer, H. Welling, and W. Ertmer, Graefe's Arch. Clin. Exp. Ophthalmol. **238**, 33 (2000).
[14]M. J. Booth and T. Wilson, J. Biomed. Opt. **6**, 266 (2001).
[15]P. S. Tsai, N. Nishimura, E. J. Yoder, E. M. Dolnick, G. A. White, and D. Kleinfeld, in *In Vivo Optical Imaging of Brain Function*, edited by R. D. Frostig (CRC, Boca Raton, 2002), pp. 113–171.
[16]Q.-T. Nguyen, P. S. Tsai, and D. Kleinfeld, J. Neurosci. Methods **156**, 351 (2006).
[17]P. S. Tsai, B. Friedman, A. I. Ifarraguerri, B. D. Thompson, V. Lev-Ram, C. B. Schaffer, Q. Xiong, R. Y. Tsien, J. A. Squier, and D. Kleinfeld, Neuron **39**, 27 (2003).
[18]V. V. Tuchin, I. L. Maksimova, D. A. Zimnyakov, I. L. Kon, A. H. Mavlyutov, and A. A. Mishin, J. Biomed. Opt. **2**, 401 (1997).
[19]G. Vargas, K. F. Chan, S. L. Thomsen, and A. J. Welch, Lasers Surg. Med. **29**, 213 (2001).
[20]T. Misgeld, M. Kerschensteiner, F. M. Bareyre, R. W. Burgess, and J. W. Lichtman, Nat. Methods **4**, 559 (2007).
[21]L. D. Landau and E. M. Lifshitz, *Theory of Elasticity* (Pergamon, Oxford, 1959), 7, 51.
[22]M. J. Booth, M. A. A. Neil, R. Juskaitis, and T. Wilson, Proc. Natl. Acad. Sci. U.S.A. **99**, 5788 (2002).
[23]L. Sherman, J. Y. Ye, O. Albert, and T. B. Norris, J. Microsc. **206**, 65 (2002).
[24]M. Rueckel, J. A. Mack-Bucher, and W. Denk, Proc. Natl. Acad. Sci. U.S.A. **103**, 17137 (2006).
[25]T. L. Kelly and J. Munch, Appl. Opt. **37**, 5184 (1998).